

PROMPT HIGH-ENERGY EMISSION FROM PROTON-DOMINATED GAMMA-RAY BURSTS

KATSUAKI ASANO¹, SUSUMU INOUE², AND PETER MÉSZÁROS³

¹ Interactive Research Center of Science, Tokyo Institute of Technology, 2-12-1 Ookayama, Meguro-ku, Tokyo 152-8550, Japan; asano@phys.titech.ac.jp

² Department of Physics, Kyoto University, Oiwake-cho, Kitashirakawa, Sakyo-ku, Kyoto 606-8502, Japan; inoue@tap.scphys.kyoto-u.ac.jp

³ Department of Astronomy & Astrophysics; Department of Physics; Center for Particle Astrophysics; Pennsylvania State University, University Park, PA 16802, USA; nnp@astro.psu.edu

Received 2008 July 7; accepted 2009 April 30; published 2009 June 17

ABSTRACT

The prompt emission of gamma-ray bursts (GRBs) is widely thought to be radiation from accelerated electrons, but an appreciably larger amount of energy could be carried by accelerated protons, particularly if GRBs are the sources of ultra-high-energy cosmic rays (UHECRs). We model the expected photon spectra for such “proton-dominated” GRBs in the internal shock scenario through Monte Carlo simulations, accounting for various processes related to high-energy electrons and protons. Besides proton and muon synchrotron components, emission from photomeson-induced secondary pair cascades becomes crucial, generally enhancing the GeV–TeV and/or eV–keV photons and offering a signature of UHE protons. In some cases, it can overwhelm the primary electron component and result in GRBs peaking in the 10 MeV–1 GeV range, which may be relevant to some bursts discussed in a recent re-analysis of EGRET TASC data. The dependence of the spectra on key quantities such as the bulk Lorentz factor, magnetic field, and proton-to-electron ratio is nontrivial due to the nonlinear nature of cascading and the interplay of electron- and proton-induced components. Observations by *Fermi*, ground-based telescopes, and other facilities should test these expectations and provide critical constraints on the proton acceleration efficiency.

Key words: cosmic rays – gamma rays: bursts – gamma rays: theory – radiation mechanisms: non-thermal

1. INTRODUCTION

The prompt emission of gamma-ray bursts (GRBs) is believed to arise from ultrarelativistic outflows with bulk Lorentz factors $\Gamma \gtrsim 100$ (see, e.g., reviews by Piran 2005; Mészáros 2006). In the popular internal shock model, collisions among inhomogeneities within the flow lead to formation of shocks that convert a fraction of the bulk kinetic energy into Fermi-accelerated relativistic electrons, whose synchrotron emission powers the observed MeV-band gamma rays (Rees & Mészáros 1994). Initially, most of the kinetic energy as well as the internal energy generated via shock dissipation are likely carried by protons, so such models entail the operation of a physical mechanism that transfers energy from protons to electrons on sufficiently short timescales. This presumably occurs via collective electromagnetic processes, as simple Coulomb collisions may be too slow. A general problem in collisionless shock theory and GRB models in particular is that this mechanism is poorly understood, and one must frequently resort to a phenomenological parameterization. In view of the large observed energy in MeV gamma rays, the efficiency of proton-to-electron energy transfer is usually considered to be high. However, this is by no means physically guaranteed. In the case of supernova remnant shocks, the total energy in accelerated electrons is often constrained observationally to be much less than in protons (e.g., Aharonian et al. 2006). Since we do not yet understand the nature and total energy budget of the central engine, we cannot readily exclude the possibility that GRBs actually contain a significantly larger amount of energy in protons compared to that radiated by the accelerated electrons.

Furthermore, a natural expectation is that the shocked protons are also Fermi accelerated. The physical conditions in internal shocks may allow maximum energies $\gtrsim 10^{20}$ eV, so GRBs are potential sources of the observed ultra-high-energy cosmic rays (UHECRs; Waxman 1995; Vietri 1995; Milgrom & Usov

1996). The total energy in accelerated protons that must be supplied per burst depends on a number of uncertain factors (see also Appendix B of Murase et al. (2008)). The required local UHECR emissivity at proton energy $\varepsilon_p \sim 10^{19}$ eV is $\varepsilon_p^2 d\dot{N}_p/d\varepsilon_p \simeq 0.8 \times 10^{44}$ erg Mpc⁻³ yr⁻¹ (Waxman & Bahcall 1998; Dermer 2007). Post-*SWIFT* estimates of the local rate of long GRBs range from 0.2–1 Gpc⁻³ yr⁻¹ if the GRB rate is proportional to the star formation rate, down to ~ 0.05 Gpc⁻³ yr⁻¹ if the GRB rate evolves more strongly with redshift, which may be observationally favored (e.g., Daigne et al. 2006; Le & Dermer 2007; Guetta & Piran 2007). Assuming a power-law proton spectrum with index $p_p = 2$, the necessary isotropic-equivalent energy per burst in accelerated protons integrated over $\varepsilon_p \sim 10^9$ – 10^{20} eV is $E_p \sim 2 \times 10^{54}$ – 3×10^{55} erg, which is approximately independent of the actual beaming factor. Steeper spectra and hence even larger E_p are called for if GRBs also contribute significantly to cosmic rays (CRs) below 10^{19} eV (Wick et al. 2004). To be compared is the corresponding energy in accelerated electrons E_e , which can be roughly equated with the observed, isotropic-equivalent MeV gamma-ray energy $E_{\gamma, \text{iso}}$, typically $\sim 10^{53}$ erg and up to $\sim 10^{54}$ erg in the 1– 10^4 keV rest-frame band (Kocevski & Butler 2008). Thus, in order for GRBs to be viable sources of UHECRs, the latest observations point to a highly proton-dominated energy budget, $E_p/E_e \gtrsim 10$ – 100 . The observed heterogeneity of GRBs also suggests that not all bursts may be equally efficient UHECR accelerators, in which case even higher E_p/E_e may be warranted for a subset of the bursts.

It is therefore of great interest whether such “proton-dominated” GRBs can be diagnosed observationally. A promising window is GeV–TeV gamma rays, where distinctive signatures of UHE proton acceleration may show up, such as synchrotron emission from protons, muons or secondary particles injected via photomeson interactions (e.g., Vietri 1997; Böttcher & Dermer 1998; Gupta & Zhang 2007; Asano & Inoue 2007, hereafter AI07).

AI07 recently undertook a detailed investigation of such emission processes utilizing a comprehensive Monte Carlo code. However, having assumed that the accelerated protons do not carry excessive extra energy, their study was restricted to $E_p/E_e = 1$. In view of the above possibilities, here we follow and extend the work of AI07 to $E_p/E_e > 1$. The results, which are often qualitatively and drastically different from AI07, are discussed in relation to existing and upcoming observations. Note that high-energy emission from proton-dominated GRBs has been discussed previously in different contexts (e.g., Totani 1998; Asano & Takahara 2003).

After a recap of our formulation in Section 2, we discuss the results and their observational implications in Sections 3 and 4, respectively, and conclude in Section 5.

2. MODEL AND METHODS

We briefly summarize the model and methods of AI07, which should be consulted for more details. In accord with the internal shock paradigm, the emitting region corresponding to an individual pulse in the prompt light curve is taken to be a homogeneous shell expanding with Γ at radii R from the central engine. The comoving width of the shell is $l = R/\Gamma$ and the pulse timescale in the observer frame is $\Delta t = R/\Gamma^2 c$, as long as R exceeds the shell spreading radius (Mészáros et al. 1993), which is always the case here. Shock dynamics and time variability are not explicitly treated, so our results should be interpreted as the time-averaged spectra for each pulse.

With given injection of accelerated electrons and protons in magnetic field B , we solve self-consistently for the distribution of particles and photons in the shell using Monte Carlo techniques. The time steps are always taken to be sufficiently shorter than the particle cooling timescales (Asano 2005). In addition to synchrotron and inverse Compton (IC) emission from all particles, our code includes synchrotron self-absorption, cascade processes with photon–photon ($\gamma\gamma$) production of electron–positron pairs (e^\pm), and Klein–Nishina regime Compton scattering, as well as proton-induced processes such as photomeson ($p\gamma$) interactions and secondary pion, muon, and pair injection. We adopt experimental results for the cross sections of $p\gamma \rightarrow n\pi^+$, $p\pi^0$, $n\pi^+\pi^0$, and $p\pi^+\pi^-$, while $p\gamma \rightarrow p\pi^0\pi^0$ is neglected in view of its small cross section. In case the primary proton is converted to a neutron, we assume that it continues to interact with photons in the shell during the comoving expansion timescale $t_{\text{exp}} = l/c$. We do not account for the minor contribution from neutron-decay electrons (Razzaque & Mészáros 2006). More details on the treatment of meson production and their decay products can be found in Asano (2005) and Asano & Nagataki (2006).

Furthermore, we now account for the Bethe–Heitler (BH) pair production process ($p\gamma \rightarrow pe^+e^-$), whose cross section and inelasticity are taken from Chodorowski et al. (1992). In the present context, the proton energy loss is always dominated by photopion production, and the huge compactness of GRBs implies that the resultant electromagnetic cascade emission is not very sensitive to the details of particle injection at high energies. Thus, compared to cases neglecting the BH process, we find that its inclusion here only leads to modest enhancements of the secondary photon emission, by at most a few tens of percent.

Primary electrons with total energy density U_e are injected with a power-law distribution $n_e(\gamma_e) \propto \gamma_e^{-p_e}$ in the range of Lorentz factors $\gamma_{e,\text{min}} \leq \gamma_e \leq \gamma_{e,\text{max}}$. The balance of Fermi acceleration and radiative cooling timescales gives $\gamma_{e,\text{max}}$.

Likewise, protons with total energy density U_p are injected with a distribution $n_p(\gamma_p) \propto \gamma_p^{-p_p}$ in the range $\gamma_{p,\text{min}} \leq \gamma_p \leq \gamma_{p,\text{max}}$. We obtain $\gamma_{p,\text{max}}$ by equating $t_{\text{acc}} = \gamma_p m_p c^2 / e B c$, the Fermi acceleration time in relativistic shocks, to $\min(t_{\text{exp}}, t_{\text{loss}})$, where t_{loss} is the energy loss time due to synchrotron, IC, and $p\gamma$ cooling (Asano 2005). In mildly relativistic internal shocks, $\gamma_{p,\text{min}}$ should be of order unity; here we take $\gamma_{p,\text{min}} = 10$.

The injection index for electrons is fiducially chosen to be $p_e = 2.5$, implying $\beta \simeq 2.25$ for the spectral index above the synchrotron peak energy. This is consistent with the mean of the β values measured by BATSE, albeit with a considerable dispersion, from $\beta \lesssim 1.5$ to $\beta \gtrsim 3.0$ (Preece et al. 2000; Kaneko et al. 2006). For protons, our fiducial index is $p_p = 2.0$, appropriate when GRBs contribute to UHECRs only above 10^{19} eV (Waxman & Bahcall 1998); steeper spectra would increase still the energy demands. Note that the values of p_e and p_p relevant to our results each correspond to very different energy ranges: GeV–TeV for electrons and 10–100 PeV for protons in the comoving frame. Although the injection spectra for the two species are expected to be the same at low energies where their gyroradii overlap, $p_e > p_p$ may be effectively realized if the proton spectrum covering 7–8 decades in energy deviates from a pure power law and becomes concave. This may plausibly occur due to (1) nontrivial geometry and wavelength distribution of magnetic turbulence at the shock (Niemiec et al. 2006), (2) nonlinear back reaction of CR pressure on the shock structure (Baring & Kirk 1991; Malkov & Drury 2001), or (3) superposition of preexisting and newly injected particles originating from different regions in the outflow (Bosnjak et al. 2008). Nevertheless, in view of the observed spread in β and the uncertainties associated with obtaining time-integrated spectra, we also discuss cases with $p_e = p_p$ in Section 3.2.

Some combinations of the remaining parameters are constrained so as to reproduce typically observed properties of the MeV emission. For given B and Γ , $\gamma_{e,\text{min}}$ is chosen such that the observed synchrotron peak energy for nearby bursts is $\varepsilon_{\text{pk}} = \Gamma \gamma_{e,\text{min}}^2 \hbar e B / m_e c \simeq 300$ keV. Since the fast-cooling, primary electrons radiate away most of their energy as MeV photons within Δt , $E_e = (4\pi \Gamma^2 R^2 c \Delta t) U_e \simeq (4\pi R^3) U_e$ can be identified with E_{sh} , the observable, isotropic-equivalent MeV pulse energy.

Instead of U_e , U_p , and $U_B = B^2/8\pi$, hereafter we use ϵ_e , ϵ_p , and ϵ_B , the conventional parameterization of the corresponding energies as fractions of the shock-dissipated internal energy (e.g., Mészáros 2006). Thus, $\epsilon_B/\epsilon_e = U_B/U_e$ and $\epsilon_p/\epsilon_e = U_p/U_e = E_p/E_e$. In place of R , we choose the observable Δt as a parameter and set $\Delta t = 0.1$ s for simplicity. Below we only show the spectra corresponding to single pulses. For bursts composed of N similar pulses, the duration-integrated energy would be simply N times larger, $E_{\gamma,\text{iso}} = N E_{\text{sh}}$. The set of parameters are then Δt , E_{sh} , Γ , ϵ_B/ϵ_e , and ϵ_p/ϵ_e . All spectra are plotted as observed fluence versus photon energy, assuming a GRB redshift $z = 0.1$. Spectral attenuation by intergalactic $\gamma\gamma$ absorption is neglected.

3. RESULTS

3.1. Fiducial Spectral Indices

First we discuss different cases with our fiducial values of $p_e = 2.5$ and $p_p = 2.0$. As mentioned above, ε_{pk} is chosen to have the typically observed value of 300 keV. Prompt emission spectra of single pulses for $E_{\text{sh}} = 10^{51}$ erg, $\Gamma = 300$, $\epsilon_B/\epsilon_e = 1$, and varying $\epsilon_p/\epsilon_e = 10$ –100 are shown in Figure 1. The sharp

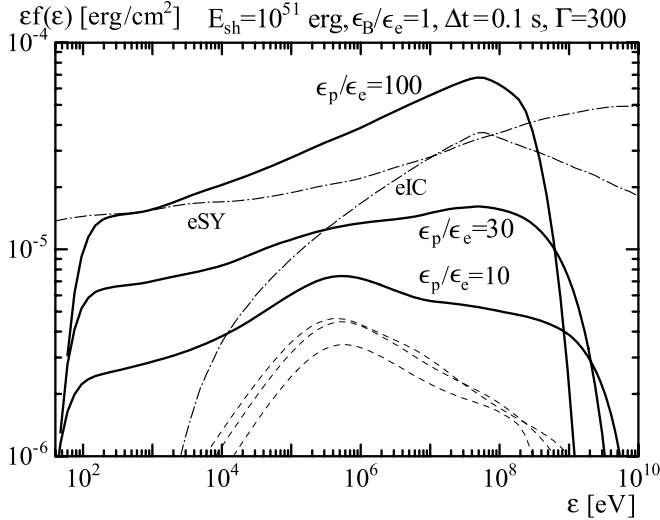


Figure 1. Single pulse, prompt photon spectra for varying ϵ_p/ϵ_e as labeled. Other parameters are marked above the figure. Dashed curves denote the primary contribution only, whose peak flux decreases with ϵ_p . Dot-dashed curves denote separately the electron synchrotron (labeled eSY) and inverse Compton (eIC) components without $\gamma\gamma$ -absorption effects for $\epsilon_p/\epsilon_e = 100$.

spectral cutoffs at low and high energies are due to synchrotron self-absorption and $\gamma\gamma$ absorption, respectively. This applies to all spectra below when such sharp cutoffs are seen. Most remarkable is the prominent e^\pm cascade component, i.e., synchrotron and IC emission from secondary e^\pm triggered by $p\gamma$ interactions of UHE protons with low-energy photons. For the lower range of ϵ_p/ϵ_e , primary synchrotron photons constitute the main $p\gamma$ target. However, as the proton content increases, the target photons become dominated by synchrotron emission from the low-energy part of the secondary e^\pm themselves. The dependence of the spectra on ϵ_p/ϵ_e is therefore nonlinear and not simply proportional, as apparent in Figure 1. The secondary photons also affect the primary synchrotron component (dashed curves in Figure 1) through enhanced IC cooling, even though the injection distribution is unchanged.

In general, cascade emission significantly hardens the high-energy spectra. Since secondary e^\pm with Lorentz factors $< \gamma_{e,\min}$ can be injected in the cascade, it can also give rise to excess UV-to-X-ray emission lying above the extrapolation of the sub-MeV spectra, as seen for $\epsilon_p/\epsilon_e = 10$ –30 in Figure 1. The entire spectra thus tend to become flat in $\epsilon f(\epsilon)$.

The case of $\epsilon_p/\epsilon_e = 100$ is drastically different. Here, the proton-induced secondary emission totally overwhelms any primary electron component, resulting in a hard spectrum peaking at 10–100 MeV. Although approximately a single power law between 100 eV and 30 MeV, in fact it comprises two emission processes by secondary e^\pm , mainly synchrotron \lesssim MeV and IC \gtrsim MeV (dot-dashed curves in Figure 1). Despite $\epsilon_B/\epsilon_e = 1$, IC can dominate over synchrotron since the energy density of secondary e^\pm exceeds both U_B and U_e .

The comoving photon density n_γ is decisive for both (1) the $\gamma\gamma$ optical depth $\tau_{\gamma\gamma}$ and hence the $\gamma\gamma$ cutoff energy $\epsilon_{\gamma\gamma}$, and (2) the efficiency of $p\gamma$ interactions and hence the secondary cascade emission. Figure 2 displays single pulse spectra for $\Gamma = 300$, $\epsilon_B/\epsilon_e = 1$, $\epsilon_p/\epsilon_e = 10$, and varying pulse energies $E_{\text{sh}} = 10^{49}$ – 10^{51} erg. Higher E_{sh} implies higher n_γ , and consequently stronger $p\gamma$ components as well as lower $\epsilon_{\gamma\gamma}$. Since $n_\gamma \propto \Gamma^{-5}$ with other parameters fixed, varying Γ has larger effects. Shown in Figure 3 are single pulse spectra for

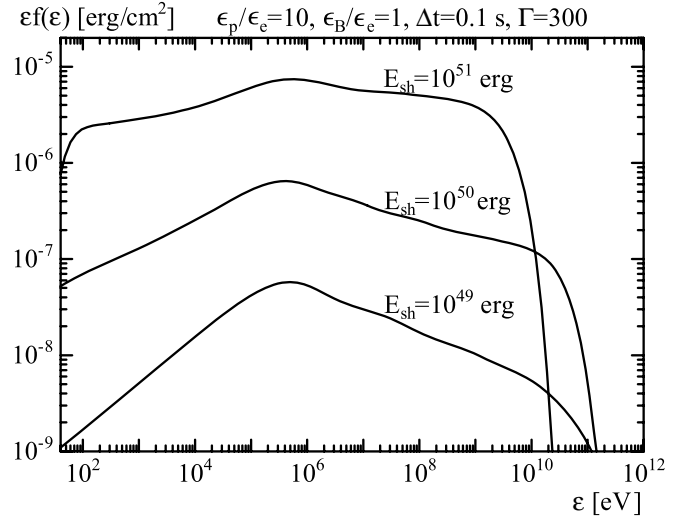


Figure 2. Single pulse, prompt photon spectra for varying E_{sh} as labeled. Other parameters are marked above the figure.

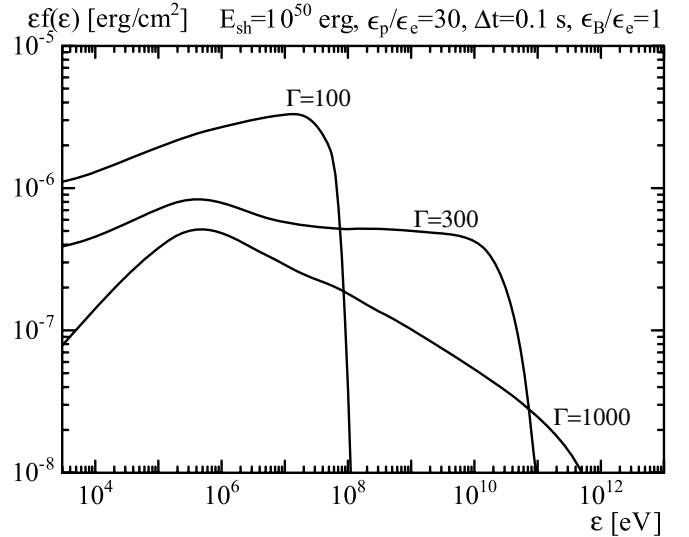


Figure 3. Single pulse, prompt photon spectra for varying Γ as labeled. Other parameters are marked above the figure.

$E_{\text{sh}} = 10^{50}$ erg, $\epsilon_B/\epsilon_e = 1$, $\epsilon_p/\epsilon_e = 30$, and $\Gamma = 100$ –1000. $\Gamma = 100$ allows a high ϵ_{pk} , cascade-dominated spectrum, even though ϵ_p/ϵ_e is three times less than the analogous case in Figure 1. Increasing Γ leads to higher maximum energies and less cascade contribution. The spectral hardening $\gtrsim 0.1$ GeV for $\Gamma = 300$ and $\gtrsim 10$ GeV for $\Gamma = 1000$ is due to secondary IC.

Thus high proton dominance does not always result in conspicuous proton-induced emission if Γ is sufficiently high. Conversely, the absence of hard, high-energy components does not necessary rule out proton-dominated GRBs. In fact, the condition most favorable for contributing to UHECRs is that they escape the source with minimal $p\gamma$ losses, which corresponds roughly to the criterion $\Gamma \gtrsim 300(\Delta t/0.1 \text{ s})^{-0.3}(E_{\text{sh}}/10^{51} \text{ erg})^{0.2}$ in our model (AI07). On the other hand, Γ can be observationally constrained through its strong influence on $\epsilon_{\gamma\gamma}$ (e.g., Lithwick & Sari 2001; AI07). Since the pulse energy E_{sh} and timescale Δt are also measurable, we may hope to identify bursts where $p\gamma$ losses are likely to be efficient, and then constrain ϵ_p/ϵ_e from the high-energy spectra, although some degeneracy with ϵ_B/ϵ_e will remain.

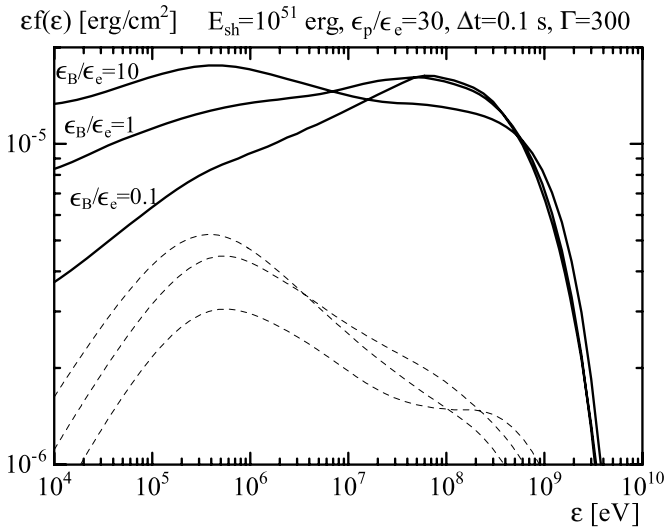


Figure 4. Single pulse, prompt photon spectra for varying ϵ_B/ϵ_e as labeled. Other parameters are marked above the figure. Dashed curves denote the primary components only, whose peak flux decreases with ϵ_B .

Figure 4 shows single pulse spectra for $E_{\text{sh}} = 10^{51}$ erg, $\Gamma = 300$, $\epsilon_p/\epsilon_e = 30$, and varying $\epsilon_B/\epsilon_e = 0.1$ – 10 . The $\epsilon_B/\epsilon_e = 1$ case is the same as in Figure 1. Higher B causes steeper spectra with stronger secondary synchrotron relative to secondary IC, while lower B is vice versa and produces a 100 MeV peak spectrum. However, the dependence on B can also be nontrivial. In Figure 5, we show spectra for $E_{\text{sh}} = 10^{51}$ erg, $\Gamma = 1000$, $\epsilon_p/\epsilon_e = 100$, and varying $\epsilon_B/\epsilon_e = 0.1$ – 100 (note that $\epsilon_B/\epsilon_p \leq 1$). The higher Γ allows spectra extending into the TeV regime, but renders $p\gamma$ processes inefficient despite the high proton dominance. All cases exhibit spectral bumps around 0.1–1 TeV, but their origins are quite different. For $\epsilon_B/\epsilon_e \lesssim 1$, this is due to secondary e^\pm IC, which is weaker for higher B . However, when $\epsilon_B/\epsilon_e \gtrsim 10$, the bump is stronger again, owing to the appearance of synchrotron emission from protons and muons, their ratio being roughly 2–1 for $\epsilon_B/\epsilon_e = 10$ (dot-dashed curves in Figure 5). For $\epsilon_B/\epsilon_e = 100$, we obtain a pronounced proton synchrotron TeV peak, as well as enhanced emission at lower energies from synchrotron radiation by e^\pm produced via $\gamma\gamma$ absorption.

3.2. Equal Proton and Electron Indices

We now consider situations with $p_e = p_p$, as would occur if the proton spectrum was a single power law over its entire energy range. Similar to the above, Figure 6 testifies that the spectrum for $\epsilon_p/\epsilon_e = 30$ and $p_e = p_p = 2.0$ can result in a hard GRB with photon index ~ 2 up to 10 GeV. It is interesting to note that in such cases, the spectral shape around the MeV peak alone may not always reveal the correct value of p_e . However, for $p_e = p_p = 2.2$, the fraction of UHE protons and the associated cascade emission is greatly diminished, except for a slight distortion of the spectrum above 100 MeV. The proton contribution becomes totally negligible for $p_e = p_p = 2.5$, for which neither UHECRs nor neutrinos are significantly generated at any rate.

4. OBSERVATIONAL IMPLICATIONS

A unique property of proton-dominated GRBs is that their photon spectra can sometimes manifest very high peak energies in the 10 MeV–1 GeV range due to $p\gamma$ cascade emission

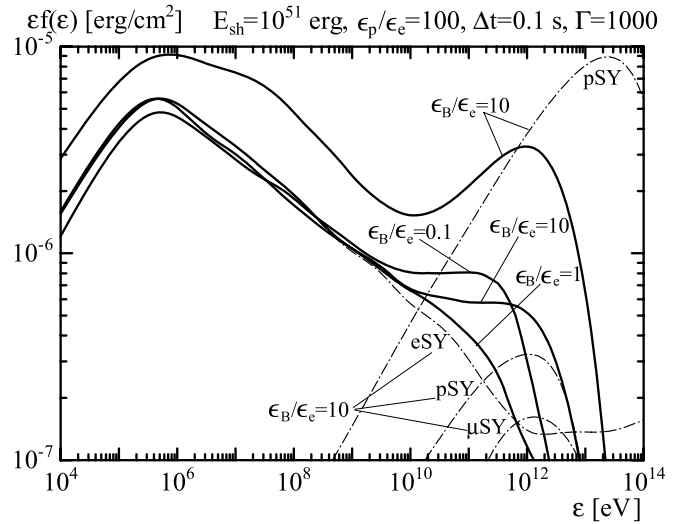


Figure 5. Single pulse, prompt photon spectra varying ϵ_B/ϵ_e as labeled. Other parameters are marked above the figure. Dot-dashed curves denote separately the electron synchrotron (eSY), proton synchrotron (pSY), and muon synchrotron (μ SY) components without $\gamma\gamma$ -absorption effects for $\epsilon_B/\epsilon_e = 10$ and 100.

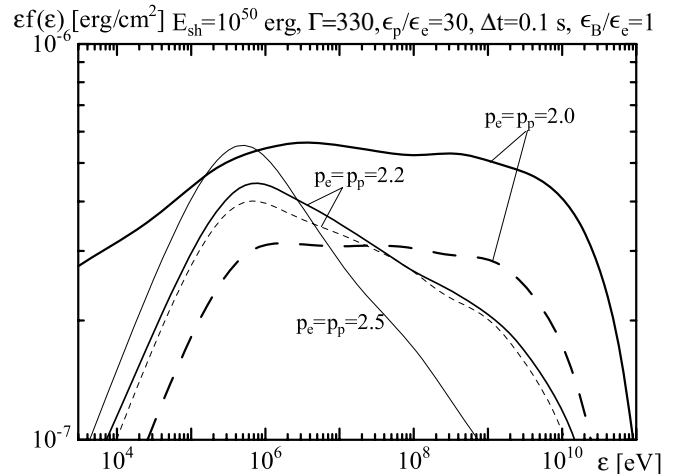


Figure 6. Single pulse, prompt photon spectra for varying values of $p_e = p_p$ as labeled. Other parameters are marked above the figure. Thick and thin dashed curves denote the primary components only, for $p_e = p_p = 2.0$ and 2.2, respectively.

(Figures 1, 3, 4, and 6). This seems at variance with commonly observed values of $\epsilon_{\text{pk}} \sim 0.1$ – 1 MeV (Kaneko et al. 2006). However, through a recent re-analysis of EGRET TASC data, Kaneko et al. (2008) reported a GRB with apparently very high $\epsilon_{\text{pk}} > 170$ MeV, as well as a few others with significant high-energy excess (see also González et al. 2003). Some studies have also indicated potential observational biases against BATSE detections of high ϵ_{pk} (Lloyd & Petrosian 1999). At this moment, it is unclear how often such high ϵ_{pk} bursts occur, and whether they are relevant to the proton-dominated cases discussed here, or simply reflect a primary synchrotron peak energy that is much higher than average (rather than the values we have assumed here). In any case, the existence and nature of such bursts will be definitively probed through ongoing observations by *Fermi* (Omodei 2006) and *AGILE* (Longo et al. 2007). Note that it is also conceivable that some GRBs possess conservative proton energies, say $E_p \sim 10^{53}$ erg, but with $E_p/E_e \gg 1$ so that the MeV emission is relatively weak. Even if unimportant

for UHECRs (Section 1), new generation satellites should also probe such MeV-weak bursts.

The $p\gamma$ cascade can also induce excess low-energy emission (Figures 1, 2, and 4), which do not seem typical of known GRBs. However, they may be relevant for some BATSE bursts with soft excess components (Preece et al. 1996), or possibly a fraction of the X-ray rich GRBs (Sakamoto et al. 2005). *Fermi* and *AGILE* observations of the accompanying high-energy excess will provide a test.

TeV detections of GRBs have yet to be achieved (e.g., Atkins et al. 2005; Albert et al. 2007; Horan et al. 2007; Aharonian et al. 2009), but some of the components discussed above may be eventually observed by current ground-based facilities such as MAGIC (II), HESS (II), VERITAS, CANGAROO III, or the future projects CTA, AGIS, HAWC, etc. For example, MAGIC may detect the luminous proton synchrotron emission for $\epsilon_B/\epsilon_e = 100$ in Figure 5 at 0.1 TeV beyond $z \sim 1$, assuming $E_{\gamma, \text{iso}} = 10^{53}$ erg and the latest estimates of intergalactic $\gamma\gamma$ absorption (Albert et al. 2008).

Distinguishing between primary electron IC and proton-induced emission components may not be easy from the spectral shape alone. However, since the synchrotron and/or photomeson cooling timescales for UHE protons are considerably longer than the cooling timescales for GeV–TeV emitting primary electrons, we can expect important differences in their variability properties, which should provide further observational clues. Although this work was limited to time-averaged pulse spectra, a desirable next step is to perform explicitly time-dependent calculations.

5. CONCLUSIONS AND OUTLOOK

Proton-dominated GRBs are motivated by physical considerations of particle acceleration in collisionless shocks, as well as their potential to be the origin of UHECRs. In GRB UHECR scenarios, the spectral index for protons at UHE must generally be harder than the typical indices for electrons emitting in the multi-MeV range, which may be possible depending on the physics of particle acceleration, cooling, and/or shock formation, as discussed in Section 2. Characteristic emission signatures can then result, such as high peak energy bursts and/or excess low-energy emission from photomeson-triggered pair cascades, or luminous spectral bumps from proton synchrotron emission. If the indices for electrons and protons at the respective energies are equal, proton-related components may still be visible as long as the index $\lesssim 2.2$, but not for steeper spectra. Through detailed observations of spectra and variability, we may hope to disentangle the proton-induced components from the competing emission process of IC from primary electrons.

Other observable consequences of proton-dominated GRBs may include contributions to Galactic CRs (e.g., Wick et al. 2004) and the diffuse high-energy neutrino background (e.g., Murase 2007).

We note that if some GRBs actually emit stronger GeV–TeV components than previously expected as discussed here, they could play an increased role in probing high- z intergalactic

radiation fields (S. Inoue et al. 2009, in preparation) as well as intergalactic magnetic fields (Ichiki et al. 2008, and references therein).

We thank Chuck Dermer for very informative correspondence, and Kohta Murase for valuable comments. Support is acknowledged from NSF PHY 0757155, NASA NNX08AL40G, Grants-in-Aid for Scientific Research Nos. 19047004 and 19540283, as well as the Global COE Program “The Next Generation of Physics, Spun from Universality and Emergence” from the Ministry of E.C.S.S.T. (MEXT) of Japan.

REFERENCES

- Aharonian, F. A., et al. 2006, *A&A*, 449, 223
 Aharonian, F. A., et al. 2009, *A&A*, 495, 505
 Albert, J., et al. 2007, *ApJ*, 667, 358
 Albert, J., et al. 2008, *Science*, 320, 1752
 Asano, K. 2005, *ApJ*, 623, 967
 Asano, K., & Inoue, S. 2007, *ApJ*, 671, 645 (AI07)
 Asano, K., & Nagataki, S. 2006, *ApJ*, 640, L9
 Asano, K., & Takahara, F. 2003, *PASJ*, 55, 433
 Atkins, R., et al. 2005, *ApJ*, 630, 996
 Baring, M., & Kirk, J. 1991, *A&A*, 241, 329
 Bosnjak, Z., Daigne, F., & Dubus, G. 2008, *A&A*, in press (arXiv:0811.2956)
 Böttcher, M., & Dermer, C. D. 1998, *ApJ*, 499, L131
 Chodorowski, M. J., Zdziarski, A. A., & Sikora, M. 1992, *ApJ*, 400, 181
 Daigne, F., Rossi, E., & Mochkovitch, R. 2006, *MNRAS*, 372, 1034
 Dermer, C. D. 2007, arXiv:0711.2804
 González, M. M., et al. 2003, *Nature*, 424, 749
 Guetta, D., & Piran, T. S. 2007, *J. Cosmol. Astropart. Phys.*, JCAP07(2007)003
 Gupta, N., & Zhang, B. 2007, *MNRAS*, 380, 78
 Horan, D., et al. 2007, *ApJ*, 655, 396
 Ichiki, K., Inoue, S., & Takahashi, K. 2008, *ApJ*, 682, 127
 Kaneko, Y., et al. 2006, *ApJS*, 166, 298
 Kaneko, Y., et al. 2008, *ApJ*, 677, 1168
 Kocevski, D., & Butler, N. 2008, *ApJ*, 680, 531
 Le, T., & Dermer, C. D. 2007, *ApJ*, 661, 394
 Lithwick, Y., & Sari, R. 2001, *ApJ*, 555, 540
 Lloyd, N., & Petrosian, V. 1999, *ApJ*, 511, 550
 Longo, F., et al. 2007, in AIP Conf. Proc. 906, Gamma-Ray Bursts: Prospects for *GLAST*, ed. M. Axelsson & F. Ryde (Melville, NY: AIP), 147
 Malkov, M. A., & Drury, L. O’C. 2001, *Rep. Prog. Phys.*, 64, 429
 Mészáros, P. 2006, *Rep. Prog. Phys.*, 69, 2259
 Mészáros, P., Laguna, P., & Rees, M. J. 1993, *ApJ*, 415, 181
 Milgrom, M., & Usov, V. 1996, *Astropart. Phys.*, 4, 365
 Murase, K. 2007, *Phys. Rev. D*, 76, 123001
 Murase, K., Ioka, K., Nagataki, S., & Nakamura, T. 2008, *Phys. Rev. D*, 78, 023005
 Niemiec, J., Ostrowski, M., & Pohl, M. 2006, *ApJ*, 650, 1020
 Omodei, N. 2006, in AIP Conf. Proc. 836, Gamma Ray Bursts in the *Swift* Era, ed. S. S. Holt, N. Gehrels, & J. A. Nousek (Melville, NY: AIP), 642
 Piran, T. 2005, *Rev. Mod. Phys.*, 76, 1143
 Preece, R. D., et al. 1996, *ApJ*, 473, 310
 Preece, R. D., et al. 2000, *ApJS*, 126, 19
 Razaque, S., & Mészáros, P. 2006, *J. Cosmol. Astropart. Phys.*, JCAP06(2006)006
 Rees, M. J., & Mészáros, P. 1994, *ApJ*, 430, L93
 Sakamoto, T., et al. 2005, *ApJ*, 629, 311
 Totani, T. 1998, *ApJ*, 509, L81
 Vietri, M. 1995, *ApJ*, 453, 883
 Vietri, M. 1997, *Phys. Rev. Lett.*, 78, 4328
 Waxman, E. 1995, *Phys. Rev. Lett.*, 75, 386
 Waxman, E., & Bahcall, J. 1998, *Phys. Rev. D*, 59, 023002
 Wick, S. D., Dermer, C. D., & Atoyan, A. 2004, *Astropart. Phys.*, 21, 125